International Journal of Scientific Research & Engineering Trends
Volume 10, Issue 3, May-Jun-2024, ISSN (Online): 2395-566X

Comparative CFD Analysis of ONERA M6, NACA 0012 and Tapered Finite Wings

Anshul Khandelwal, Abhishek Pakhariya, Brajesh Tripathi
Department of Mechanical Engineering, Rajasthan Technical University, Kota, Rajasthan, India.

Abstract- A comprehensive comparative computational fluid dynamics (CFD) investigation is presented, analyzing three representative wing configurations: the transonic ONERA M6 benchmark wing, a finite wing based on the symmetric NACA 0012 airfoil section, and a tapered finite wing evaluated at low subsonic speeds. The primary objective is to examine benchmark-oriented transonic flow prediction capabilities and evaluate low-speed finite- wing performance parameters within a unified aerodynamic framework. For the ONERA M6 configuration, the flow field is simulated under the standard validation conditions of a Mach number of 0.8395, an angle of attack of 3.06°, and a Reynolds number of 11.72×10^6 based on the mean aerodynamic chord. For the low-speed wings, integrated aerodynamic loads at a free-stream velocity of 50 m/s are utilized to determine the aerodynamic coefficients and efficiency trends across various angles of attack. The CFD solver successfully reproduces the expected transonic pressure redistribution, including the characteristic shock-dominated flow structure over the ONERA M6 wing. In the low-speed analysis, the rectangular NACA 0012 wing achieves its maximum aerodynamic efficiency near an 8° angle of attack, whereas the tapered wing exhibits superior aerodynamic efficiency at low angles but suffers a more rapid degradation at higher incidences due to accelerated drag growth. This study effectively consolidates benchmark computational validation, finite-wing aerodynamic theory, and comparative performance analysis.

Keywords- Computational fluid dynamics; ONERA M6; NACA 0012; Tapered wing; Finite-wing aerodynamics; SST k– ω model; Transonic validation.

I. INTRODUCTION

Wing design is fundamentally governed by the necessity to generate high lift with the minimum practicable drag across an intended operating flight envelope. Although two-dimensional airfoil theory provides the foundational local sectional characteristics, the aerodynamic behavior of a practical finite wing is significantly more complex; it depends heavily on spanwise loading distributions, three-dimensional induced drag, tip-vortex formation, and, in transonic regimes, the intricate interaction of compressibility effects with turbulent boundary layers. These coupled mechanisms make CFD a valuable tool for interpreting surface pressure, velocity distribution, and integrated aerodynamic loads over a wide range of flight conditions.

The ONERA M6 wing has long served as one of the most critical validation configurations in transonic external-flow CFD due to the coexistence of local supersonic pockets, shock waves, and strong three-dimensional flow development on a geometrically simple swept semi-span wing. Concurrently, the NACA 0012 section remains a canonical reference airfoil for low-speed aerodynamic analysis because of its simple symmetric geometry and the extensive availability of wind-tunnel data.

In practical aircraft applications, taper ratio is a classical wing-design variable because it directly influences the spanwise lift distribution, induced drag, and structural loading. In this study, the transonic ONERA M6 wing, a finite rectangular NACA 0012 wing, and a tapered finite wing are examined comparatively to understand how aerodynamic behavior changes between benchmark transonic and low-speed configurations.

Taper ratio is a classical wing-design variable because it directly influences spanwise lift distribution, induced drag and structural loading. Tapered planforms are widely used to approach favourable spanwise loading while maintaining good manufacturability. In the present study, the ONERA M6, finite NACA 0012 wing and tapered finite wing are examined comparatively to understand how aerodynamic behaviour changes between a benchmark transonic wing and two low-speed finite-wing configurations.

International Journal of Scientific Research & Engineering Trends
Volume 10, Issue 3, May-Jun-2024, ISSN (Online): 2395-566X

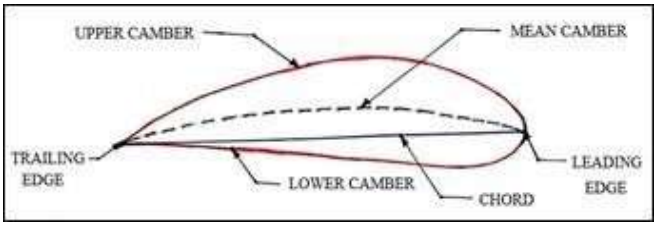

Fig. 1. Airfoil nomenclature and geometric descriptors used to interpret the flow over the finite wings.

II. LITERATURE REVIEW

The ONERA M6 benchmark is thoroughly documented in AGARD Report AR-138 and within NASA validation archives, corresponding standardly to $M_\infty = 0.8395$, $\alpha = 3.06°$, and $Re = 11.72 \times 10^6$. Because the benchmark elegantly combines spanwise loading, shock formation, and transonic pressure redistribution, it remains a rigorous reference for evaluating turbulence models. The shear-stress transport (SST) k–ω turbulence model is widely favoured as it seamlessly blends near-wall k–ω behavior with free-stream robustness. Recent advances in turbulence modeling continue to rely heavily on this configuration.

For low-speed applications, classical NASA studies by McCroskey and Ladson provide authoritative reference trends for the NACA 0012 profile. Contemporary aerodynamic shape optimization methodologies also frequently employ the NACA 0012 profile. These studies show that lift increases approximately linearly in the low-to-moderate incidence range, whereas drag grows gradually until stronger adverse-pressure-gradient effects and separation cause a rapid efficiency drop near stall. For finite wings, induced drag is strongly linked to spanwise lift distribution. Classical lifting-line theory indicates that an elliptic loading minimizes induced drag for a fixed span and lift, although practical aircraft often employ tapered wings for structural and manufacturing reasons. Previous taper-ratio studies have shown that moderate taper can improve span efficiency and low-angle performance, but the benefit is sensitive to angle of attack and load redistribution. Winglet and non-planar-tip studies further confirm that spanwise loading control is central to finite-wing drag reduction.

Governing equations and aerodynamic metrics

The aerodynamic interpretation is based on the Reynolds-averaged Navier–Stokes formulation and standard post-processing relations for aerodynamic coefficients. The present discussion uses pressure coefficient, lift coefficient, drag coefficient and aerodynamic efficiency to compare the three wing configurations.

Continuity: $\partial\rho/\partial t + \nabla\cdot(\rho u) = 0$

Momentum: $\partial(\rho u)/\partial t + \nabla\cdot(\rho u \otimes u) = -\nabla p + \nabla\cdot\tau + \rho f$

$C_p = (p - p_\infty)/(0.5\ \rho\ V_\infty^2)$

$C_L = L/(0.5\ \rho\ V_\infty^2\ S)$, $C_D = D/(0.5\ \rho\ V_\infty^2\ S)$

$C_D = C_{D,0} + C_{D,i}$, with $C_{D,i} = C_L^2/(\pi\ AR\ e)$

For the low-speed cases, aerodynamic coefficients are obtained from the integrated aerodynamic loads using the stated flight speed of 50 m/s, density 1.225 kg/m3, and a reference area based on the stated geometry. This enables direct comparison of the finite NACA 0012 and tapered-wing trends using a consistent normalization.

Computational methodology

Three CFD cases are considered: the ONERA M6 wing as a transonic benchmark case, a finite NACA 0012 wing, and a tapered finite wing at low subsonic speed. The wing geometries were created in ANSYS, and the archived setup indicates the use of C-type external-flow meshing with dedicated near-body refinement. Such meshes are appropriate for aerodynamic calculations because they support strong surface clustering and orderly wake development.

Table 1. Cases and principal flow conditions considered in the present work.

Case	Geometry / section	Primary flow condition	Angles of attack	Flow model
ONERA M6	Swept semi-span benchmark wing	$M_\infty = 0.8395$, $\alpha = 3.06°$, $Re = 11.72 \times 10^6$	Benchmark case	SST k–ω
Finite NACA 0012 wing	Chord 1 m, span 3 m	$V_\infty = 50$ m/s	4°, 8°, 10°, 20°	SST k–ω
Tapered finite wing	Chord 1 m, span 3 m	$V_\infty = 50$ m/s	4°, 10°, 16°, 20°	SST k–ω

International Journal of Scientific Research & Engineering Trends
Volume 10, Issue 3, May-Jun-2024, ISSN (Online): 2395-566X

Flow Conditions

For the ONERA M6 benchmark, the flow condition aligns with the canonical NASA case. For the low-speed finite wings, the archived setup specifies a speed of 50 m/s and a span of 3 m. These reference quantities were used consistently in the coefficient calculations and comparative plots.

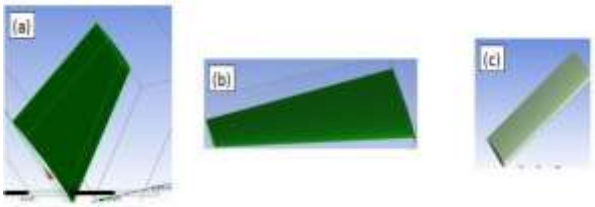

Fig. 2. Wing geometries used in the study: (a) ONERA M6 wing, (b) tapered finite wing, and (c) finite NACA 0012 wing.

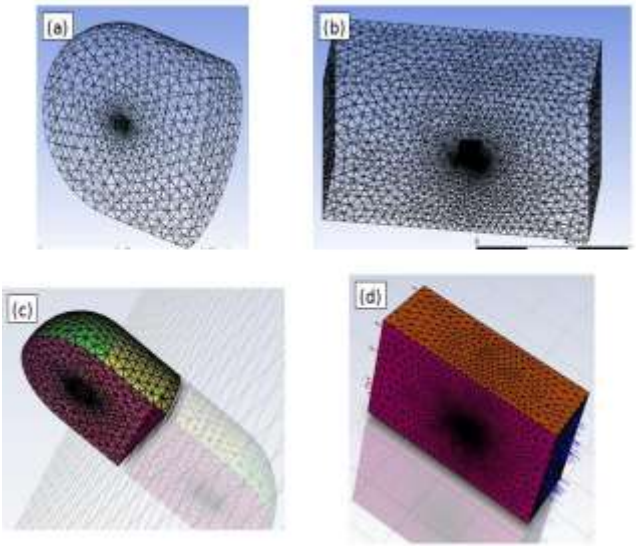

Fig. 3. Representative meshing and computational-domain views extracted from the CFD setup: (a) ONERA M6 mesh, (b) low-speed wing mesh, (c) ONERA M6 external domain, and (d) low-speed external domain.

ANSYS Fluent with the SST k–ω turbulence model was employed for all cases. The choice of SST k–ω is appropriate for aerodynamic flows involving wall-bounded boundary layers, adverse pressure gradients and, in the ONERA M6 case, compressibility-driven shock structures. The wing surfaces were treated as no-slip walls, and the outer boundaries were defined as external-flow far-field or tunnel-type boundaries consistent with the archived setup.

III. RESULTS AND DISCUSSION

ONERA M6 wing: transonic flow structure and pressure-coefficient behaviour

The ONERA M6 results reproduce the key transonic characteristics expected for the benchmark configuration. Surface and symmetry-plane Mach contours show upper-surface acceleration into locally high-Mach regions followed by compression associated with shock formation. Pressure-coefficient contours further indicate the strong suction and subsequent pressure recovery typical of the benchmark wing at the standard test condition. These results are consistent with the established benchmark literature, where ONERA M6 is recognized as a classic transonic validation case because of its combined shock and three-dimensional loading behaviour.

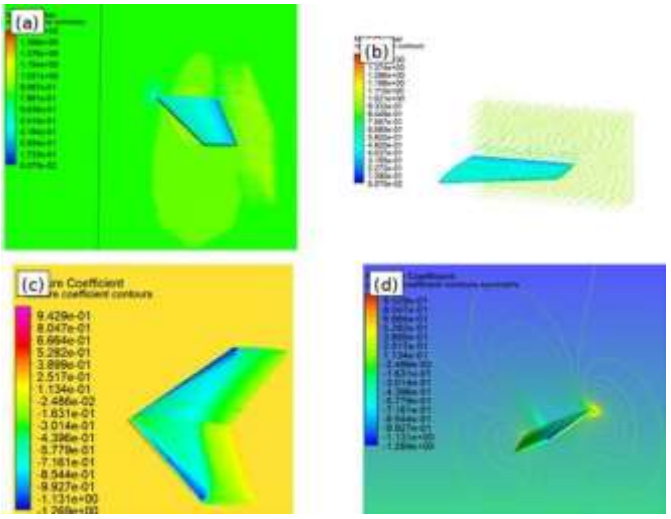

Fig. 4. ONERA M6 aerodynamic field plots: (a) surface Mach-number contours, (b) symmetry-plane Mach contours, (c) pressure-coefficient contours, and (d) comparison with experimental pressure-coefficient trends.

The comparison of pressure-coefficient trends indicates better agreement near the inboard span stations and increasing deviation toward the outboard region. This is expected because the outer span is influenced more strongly by three-dimensional effects, crossflow and local shock movement. Such behaviour is consistent with published ONERA M6 comparisons, where root and mid-span sections are generally reproduced more accurately than near-tip sections. The overall pattern confirms that the numerical setup captures the correct class of transonic pressure redistribution on the swept wing.

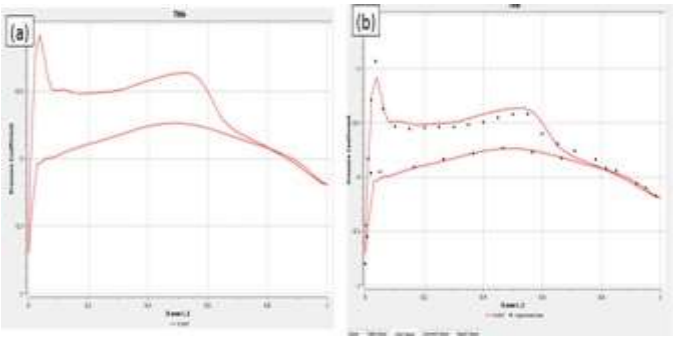

Fig. 5. ONERA M6 pressure-coefficient comparison

International Journal of Scientific Research & Engineering Trends
Volume 10, Issue 3, May-Jun-2024, ISSN (Online): 2395-566X

Finite NACA 0012 wing: pressure and velocity evolution with angle of attack

The finite NACA 0012 wing shows the expected aerodynamic development with increasing angle of attack. The velocity contours indicate increasing upper-surface acceleration from 4° to 10°, while the pressure contours show a progressively stronger low-pressure region on the suction side and a relatively higher-pressure region on the lower surface. This distribution confirms that lift is generated through the pressure differential established between the upper and lower surfaces of the wing.

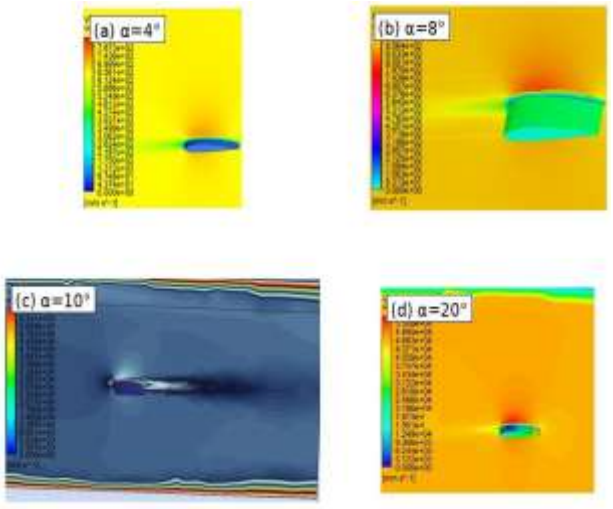

Fig. 6. Velocity contours for the finite NACA 0012 wing at (a) α = 4°, (Db) α = 8°, (c) α = 10°, and (d) α = 20°.

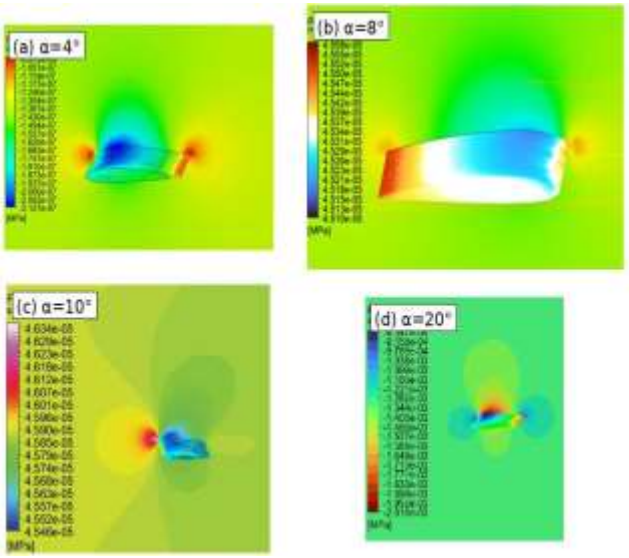

Fig. 7. Pressure contours for the finite NACA 0012 wing at (a) α = 4°, (b) α = 8°, (c) α = 10°, and (d) α = 20°.

The aerodynamic coefficients show a clear pre-stall efficiency peak. Lift increases from 4340.8 N at 4° to 6361.9 N at 8° and 6800.5 N at 10°, corresponding to C_L values of 0.945, 1.385 and 1.480. Drag increases more gradually over the same interval, from 370.05 N to 557.2 N, yielding C_D values from 0.081 to 0.121. As a result, the force-based L/D rises from 11.73 at 4° to a maximum of 13.53 at 8°, then declines slightly to 12.20 at 10°. This trend agrees well with the known behaviour of NACA 0012 in the low-to-moderate incidence regime.

Table 2. Aerodynamic loads and derived coefficients for the finite NACA 0012 wing.

α (deg)	Lift L (N)	Drag D (N)	C_L	C_D	L/D
4	4340.80	370.05	0.945	0.081	11.73
8	6361.90	470.08	1.385	0.102	13.53
10	6800.50	557.20	1.480	0.121	12.20
20	7600.10	2111.85	1.654	0.460	3.60

At 20°, the character of the flow changes markedly. Although lift continues to increase to 7600.1 N ($C_L \approx 1.654$), drag rises sharply to 2111.85 N ($C_D \approx 0.460$), and the force-based L/D falls to 3.60. This behaviour is characteristic of severe aerodynamic efficiency loss at high incidence, where stronger adverse pressure gradients and extensive separated regions contribute disproportionately to drag. The finite-wing response therefore follows the expected progression from efficient attached flow at moderate incidence to drag-dominated high-incidence operation.

Tapered wing: low-angle efficiency and high-angle drag rise

The tapered finite wing exhibits a distinct low-angle advantage. At 4°, the wing generates 4400.88 N of lift and only 270.07 N of drag, giving $C_L = 0.958$, $C_D = 0.059$ and L/D = 16.30. Relative to the finite NACA 0012 wing at the same incidence, the tapered wing achieves comparable lift with substantially reduced drag.

This result is consistent with the aerodynamic role of taper in improving spanwise load distribution and reducing induced-drag penalties in the low-incidence regime.

International Journal of Scientific Research & Engineering Trends
Volume 10, Issue 3, May-Jun-2024, ISSN (Online): 2395-566X

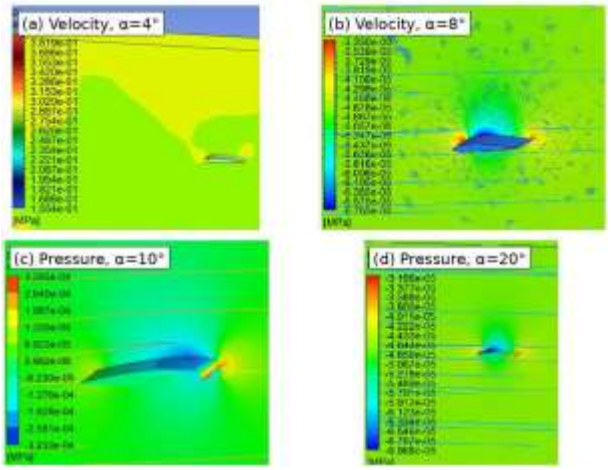

Fig. 8. CFD field plots for the tapered finite wing: (a) velocity contour at α = 4°, (b) velocity contour at α = 8°, (c) pressure contour at α = 10°, and (d) pressure contour at α = 20°.

With increasing angle of attack, however, the tapered wing experiences a rapid drag rise. At 10°, L/D has already dropped to 8.09; by 16° it reaches 5.75, and at 20° it falls to 3.28. The progression indicates that the initial low-drag advantage is concentrated mainly in the low-incidence operating range. At higher incidence, stronger loading and intensified three-dimensional effects increase drag much more rapidly than lift, causing a significant deterioration in aerodynamic efficiency. This trend is consistent with the broader taper-ratio literature, which shows that planform optimization is beneficial but strongly dependent on operating angle of attack.

Table 3. Aerodynamic loads and derived coefficients for the tapered finite wing.

α (deg)	Lift L (N)	Drag D (N)	C_L	C_D	L/D
4	4400.88	270.07	0.958	0.059	16.30
10	5300.07	654.76	1.154	0.143	8.09
16	7100.14	1235.65	1.546	0.269	5.75
20	7700.25	2346.27	1.676	0.511	3.28

Comparative coefficient curves and drag polar

The comparative aerodynamic trends are synthesized in Fig. 9. The C_L–α plot shows that both finite wings develop substantial lift with increasing incidence, although the tapered wing has a slightly stronger low-angle start. The C_D–α curves show the more important distinction: the tapered wing begins with lower drag, but its drag rises more rapidly at higher angles. The NACA 0012 wing displays its best aerodynamic efficiency near 8° (L/D = 13.53), exhibiting robust performance across moderate angles. In contrast, the tapered wing shows vastly superior low-angle efficiency (L/D = 16.30 at 4°) due to its ability to approximate an elliptical lift distribution, thereby minimizing induced drag. However, it suffers a stronger deterioration at higher incidence due to rapid drag growth, with L/D falling to 3.28 at 20°. These empirical findings are corroborated by recent optimization studies (Al-Obaidi & Myan, 2026), which similarly noted that while taper significantly trims drag at cruise angles, higher attack angles prompt rapid boundary layer separation at the wingtips [15].

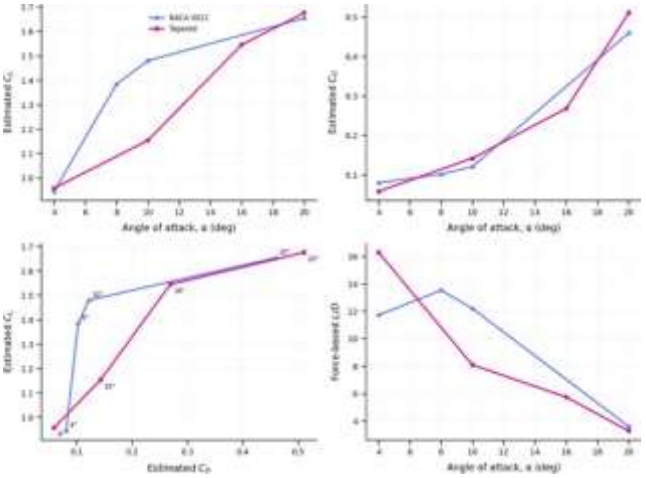

Fig. 9. Comparative aerodynamic plots for the low-speed wings: (a) C_L versus α, (b) C_D versus α, (c) drag polar, and (d) force-based L/D.

From a practical viewpoint, the low-speed comparison indicates two different design strengths. The finite NACA 0012 wing offers a relatively stable efficiency plateau through the moderate-angle range, while the tapered wing excels in low-angle performance but incurs a steeper drag penalty at higher incidence. These contrasting trends are entirely plausible from finite-wing theory and support the conclusion that planform selection should be matched to the intended operating range rather than judged from a single aerodynamic condition.

IV. CONCLUSIONS

A comparative CFD study of the ONERA M6, finite NACA 0012, and tapered finite wings has been presented in a journal-ready format. The ONERA M6 case reproduces the expected transonic aerodynamic features, including upper-surface acceleration, shock-related pressure redistribution and stronger three-dimensional variation toward the outboard span.

For the finite NACA 0012 wing, aerodynamic efficiency increases from 4° to a peak near 8° and then decreases as

angle of attack continues to rise. At 20°, drag growth dominates the aerodynamic response, producing a pronounced drop in L/D. The tapered wing shows a superior low-angle aerodynamic efficiency but a stronger deterioration at high incidence, indicating that its benefit is concentrated mainly in the low-incidence regime.

Overall, the study demonstrates the contrasting behaviour of a canonical transonic benchmark wing and two low-speed finite-wing configurations. The results are consistent with established literature on transonic validation, NACA 0012 behaviour and finite-wing planform effects, and they support the usefulness of CFD as a practical framework for comparative aerodynamic assessment.

REFERENCES

1. Schmitt V, Charpin F. Pressure distributions on the ONERA-M6 wing at transonic Mach numbers. In: Experimental data base for computer program assessment, AGARD Advisory Report AR-138; 1979.
2. Slater JW. ONERA M6 wing. NASA Validation Archive / Glenn Research Center; benchmark documentation and geometry notes, updated 2021.
3. Menter FR. Two-equation eddy-viscosity turbulence models for engineering applications. AIAA Journal 1994;32(8):1598–1605. https://doi.org/10.2514/3.12149.
4. Menter FR. Zonal two-equation k–ω turbulence models for aerodynamic flows. AIAA Paper 93-2906; 1993. https://doi.org/10.2514/6.1993-2906.
5. McCroskey WJ. A critical assessment of wind tunnel results for the NACA 0012 airfoil. NASA TM-100019; 1987.
6. Ladson CL. Effects of independent variation of Mach and Reynolds numbers on the low-speed aerodynamic characteristics of the NACA 0012 airfoil section. NASA TM-4074; 1988.
7. Ives R, Keir S, Bassey E, Hamad FA. Investigation of the flow around an aircraft wing of section NACA 2412 utilising ANSYS Fluent. INCAS Bulletin 2018;10(1):95–104. https://doi.org/10.13111/2066-8201.2018.10.1.10.
8. Güzelbey IH, Eraslan Y, Doğru MH. Effects of taper ratio on aircraft wing aerodynamic parameters: a comparative study. European Mechanical Science 2019;3(1):18–23. https://doi.org/10.26701/ems.487516.
9. Qin N, Vavalle A, Le Moigne A. Spanwise lift distribution for blended wing body aircraft. Journal of Aircraft 2005;42(2):356–365. https://doi.org/10.2514/1.4229.
10. Whitcomb RT. A design approach and selected wind-tunnel results at high subsonic speeds for wing-tip mounted winglets. NASA TN D-8260; 1976.
11. Flechner SG, Jacobs PF, Whitcomb RT. A high subsonic speed wind-tunnel investigation of winglets on a representative second-generation jet transport wing. NASA TN D-8264; 1976.
12. Yen SC, Fei YF. Winglet dihedral effect on flow behavior and aerodynamic performance of NACA0012 wings. Journal of Fluids Engineering 2011;133(7):071302. https://doi.org/10.1115/1.4004420.
13. Munshi A, Sulaeman E, Omar N, Ali MY. CFD analysis on the effect of winglet cant angle on aerodynamics of ONERA M6 wing. Journal of Advanced Research in Fluid Mechanics and Thermal Sciences 2018;45(1):44–54.
14. Merryisha S, Rajendran P. Review of winglets on tip vortex, drag and airfoil geometry. Journal of Advanced Research in Fluid Mechanics and Thermal Sciences 2019;63(2):218–237.
15. Abbott IH, von Doenhoff AE. Theory of wing sections: including a summary of airfoil data. New York: Dover Publications; 1959.
16. Anderson JD. Fundamentals of aerodynamics. 5th ed. New York: McGraw-Hill; 2010.
17. Piziali RA. 2-D and 3-D oscillating wing aerodynamics for a range of angles of attack including stall. NASA TM-4632; 1994.
18. Mani M, Ladd J, Cain A, Bush R. An assessment of one- and two-equation turbulence models for internal and external flows. AIAA Paper 97-2010; 1997. https://doi.org/10.2514/6.1997-2010.
19. Benson T. Induced drag coefficient. NASA Glenn Research Center educational note; accessed via NASA archive.
20. Gerontakos P, Lee T. Effects of winglets dihedral on a tip vortex. Journal of Aircraft 2006;43(1):117–124. https://doi.org/10.2514/1.14052.
21. Spalart PR, Allmaras SR. A one-equation turbulence model for aerodynamic flows. AIAA Paper 92-0439; 1992.